Electronic Supplementary Material (ESI) for Nanoscale Advances.

Supplementary materials

for

Ultrabright fluorescent nanothermometers

V. Kalaparthi[1,†], B. Peng[2], S.A.M. Peerzade[2], S. Palantavida[1,††], B. Maloy[3], M. E. Dokukin[1,4,5], I. Sokolov[1,2,3,]*

[1] Department of Mechanical Engineering, Department of Biomedical Engineering, Tufts University, 200 College ave., Medford, MA 02155, USA;

[2] Department of Biomedical Engineering, 4 Colby Str., Medford, MA 02155, USA.

[3] Department of Physics, Tufts University, 547 Boston ave., Medford, MA 02155, USA.

[4] Sarov Physics and Technology Institute, Sarov, Russian Federation

[5] National Research Nuclear University MEPhI, Moscow, Russian Federation

† Present address: GLOBALFOUNDRIES, 1000 River Str., Essex Junction, VT 05452, USA

†† Present address: Center for Nano and Material Sciences, Jain University, Jakkasandra, Kanakapura, Karnataka 562112 India

1. Physical dimensions of particles

The average size of the nanoparticles measured and the distribution is centered between 40-50 nm, Fig.S1a. The particle size distribution measured with the DLS method for three runs shows a similar size distribution of particles dispersed in water, Fig.S1b.

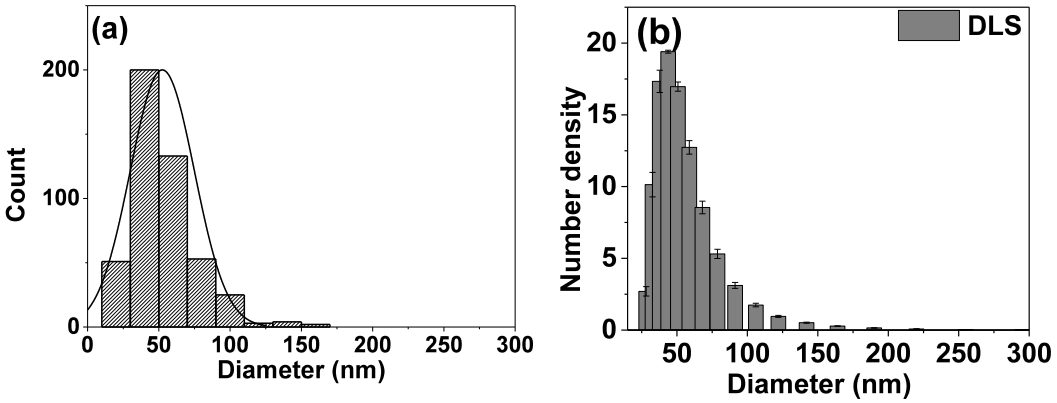

Figure S1. Physical dimensions of the nanothermometers. (a) The particle size distribution obtained from TEM images (b) particle size distribution obtained from DLS method

2. Calculation of the effective brightness of nanothermometers

To calculate the concentration of the dye molecules encapsulated inside nanothermometers, we first measure the particle concentration in water dispersion. A known volume of stock solution of nanoparticles was dried in oven at 60^{o} C for 6 hours. The mass of the particle per unit volume of the solution was found to be 0.12±0.03 mg/mL (the experiment was repeated three times; dry residue of pure water was considered as a baseline). Using the mass density of 1.6 g/cm^3 for the porous silica [1, 2], and taking the average particle size of 50 nm, one can find the number of particles in the stock solution, which is equal to 1.15x10^{12} /mL. To estimate the number of encapsulated dye molecules, UV-VIS absorbance was measured. A water dispersion of nanoparticles in the concentration of 0.71x10^{11} /mL was used to measure absorbance. One can find the concentration of both the dyes from known extinction coefficients of R6G and RhB (1.0x10^5 L/mole/cm at 525 nm for R6g and 1.2x10^5 L/mole/cm at 550 nm for RhB dye), and using the Beer–Lambert law. Here we note that such a procedure in general is applicable for free dye solutions. However, one can apply similar procedure for dye encapsulated inside the particles by subtracting the porous silica contribution from the preliminary data, which is a superposition of contribution from silica contribution and encapsulated dyes, see [3] for details. Finally, since the dye molecules are physically entrapped inside the channels, one would need to verify that the optical properties of dyes remain unaltered after encapsulation. It was done by dissolving the silica matrix with hydroftoric acid [3].

Figure S2 shows the absorbance spectrum of the nanothermometers in room temperature considered after removing(subtracting the slope) porous silica contribution . One can see the absorbance values for R6G (at 525 nm) and RhB (at 550 nm) are 0.0084 and .0093, respectively. The Beer–Lambert law translates these into the concentrations of 84 nM for R6G and 78 nM for RhB dyes inside the particles. Because this was found for the concentration 1.15×10^{12} $mL^{-1}$of 50 nm particles, each 50 nm particle contains 710 R6G and 650 RB molecules. (The estimated concentration of R6G and RhB in each particle was found to be 1.80 mM and 1.66 mM, respectively.)

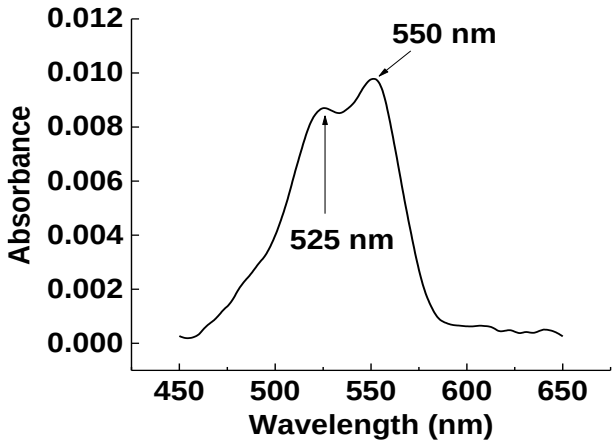

Figure S2. The absorbance spectrum of the nanothermometers in room temperature.

Using rhodamine 6G and B as the reference dyes, and measuring fluorescence coming from the solution with known concentrations of fluorescent silica particles (C_{P}) and the reference dyes (for example of rhodamine 6G, C_{R6G}), one can find the sought relative brightness of material of fluorescent particle as follows

$$\text{Relative brightness R6G} = \frac{FL_{\mathrm{P}} / C_{\mathrm{P}}}{FL_{\mathrm{R6G}} / C_{\mathrm{R6G}}} = 146, \quad \text{Relative brightness RB} = \frac{FL_{\mathrm{P}} / C_{\mathrm{P}}}{FL_{\mathrm{RB}} / C_{\mathrm{RB}}} = 1720 \tag{S1}$$

where FL_{NP} (*or* FL_{R6G} FL_{RB}) is the amount of fluorescent light coming from a suspension of the particles in water (or solution of reference R6G or RB dye). Note that fluorescence of nanoparticles was split into separate spectra of R6G and RB by deconvolution algorithm, as shown below.

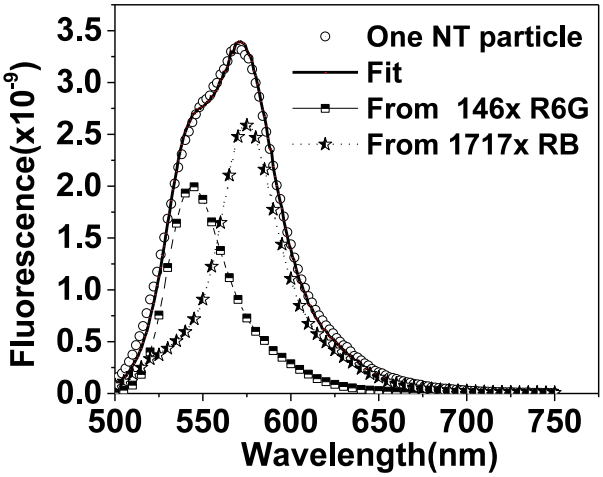

Figure S3: An example of fluorescence emission of nanothermomethers and the decoupled peaks of R6G and RB presented with respect to their relative contribution to brightness using the deconvolution algorithm. Note that this spectrum was obtained for particles as synthesized. It changes to the spectra shown in figure 3 of the main text after the initial heat treatment of the particles.

It should be noted that the particle brightness may depend on the excitation wavelength because of the presence of FRET. But as soon as the direct excitation of rhodamine B is a weak relative to rhodamine 6G ($\varepsilon_{R6G}/\varepsilon_{RB} = 3.13$ at 488 nm), this dependence is insignificant.

The number of dye molecules encapsulated are and the quantum yield of NTs with respect to R6G is 37% (0.37).

3. Calculation of the Förster distance

The Forster distance was calculated by considering the emission spectrum of R6G dye as a donor and absorbance spectrum of RB as acceptor. Their spectral characteristics (fluorescent emission

of R6G and absorbance of rhodamine B) are shown in Figure S3. The Forster distance, *Ro*, can be calculated using the following formula [4]:

$$R_0 = 0.0211 \times (\kappa^2 n^{-4} Q_D J)^{1/6} \qquad \text{(in nm)}$$

where κ^2 is the dipole orientation factor between the donor(R6G) and the acceptor(RB), n is the refractive index of the medium, Q_D is the quantum yield of the donor and J is the spectral overlap integral of the donor-acceptor pair given by the equation:

$$J = \frac{\int_0^\infty F_D(\lambda)\varepsilon_A(\lambda)\lambda^4 d\lambda}{\int_0^\infty F_D(\lambda) d\lambda} \qquad \text{(in } M^{-1}cm^{-1}\ nm^4\text{)}$$

Here $F_D(\lambda)$, $\varepsilon_A(\lambda)$ correspond to fluorescence of the donor and the extinction coefficient of acceptor, respectively , at each wavelength.

Thee overlap integral for the R6G donor and the RB acceptor pair in the wavelength range 500 nm to 650 nm was calculated to be 1.93×10^{16} $M^{-1}cm^{-1}\ nm^4$. By considering the quantum yield of donor, $Q_D = 0.95$, and refractive index of silica as 1.43 and with assumed dipole orientation factor of 2/3, the Förster distance, R_0, can be estimated as 8 nm.

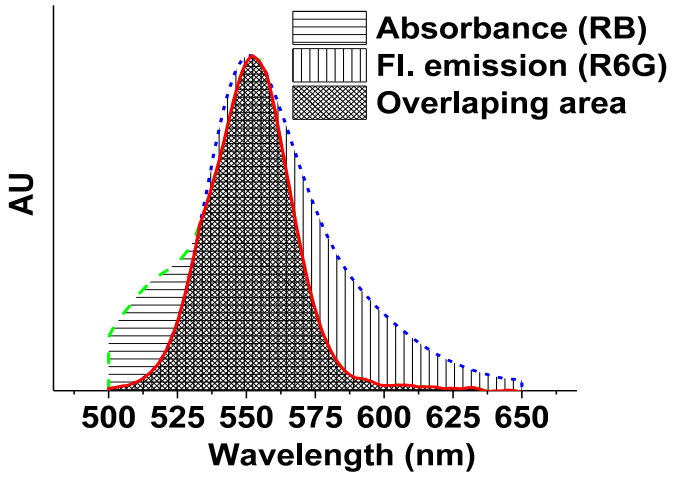

Figure S4: Emission and absorbance spectra of R6G (donar (blue line)) and RB (acceptor(green line)) is presented, respectively, with the overlapping area enclosed (redline).

4. Independence of temperature sensing of concentration of nanothermometers

The ratio of the fluorescent intensities, which is indicative of temperature, should not depend on concentration of nanothermometers. Figure S5 demonstrates such independence for fluorescence taken at multiple wavelengths.

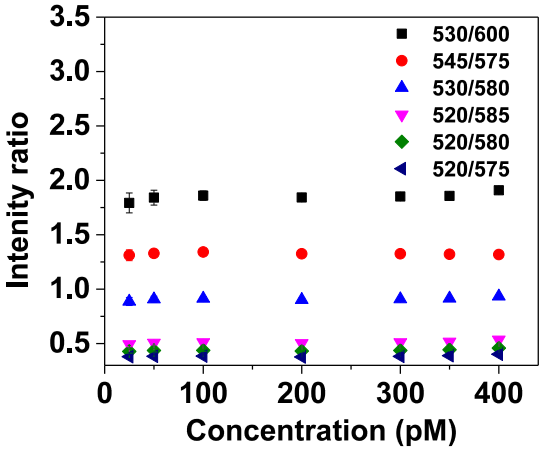

Figure S5: Intensity ratios for different wavelengths at various concentrations are presented. All experimental results presented in the main article are carried at 35 pM concentration.

5. Independence of temperature sensing of intensity of the excitation light

The ratio of the fluorescent intensities, which is indicative of temperature, should independent of intensity of the excitation light. Figure S6 demonstrates such independence for fluorescence taken at multiple wavelengths.

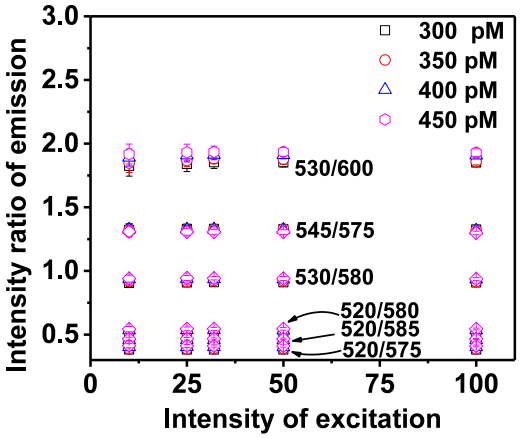

Figure S6: Intensity ratios for different wavelengths at various excitation intensity are presented. The concentration of 300 pM, 350 pM, 400 pM and 450 pM of nanothermometers in water is presented.

6. Ratiometric temperature sensing example by using fluorescent maxima of individual dyes (545 nm to 573 nm)

Figure S7 (a) shows the temperature dependence of the ratio of fluorescent intensities at 545 nm to 573 nm of the nanothermometers excited at 488 nm. One can see a fairly linear response when temperature being changed within 20-50^{o} C in steps of 5^{o} C. Similar measurements for the dye mixture solution show virtually no dependence on temperature, Fig.S7 (b). The average ratio for 40 measurements is shown (the error bar is one standard deviation). Based on this error bar one can calculate the uncertainty in temperature measurements. It is rather uniform for the range of temperatures started and found to be 1.8^{o}C.

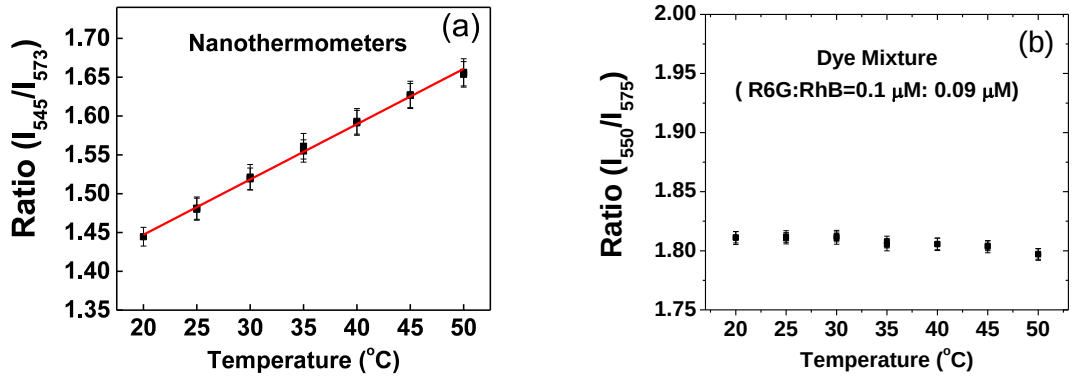

Figure S7: Temperature dependence of the ratio of fluorescent intensities for (a) nanothermometers with R6G and RhB dyes encapsulated, and (b) free dyes mixture. The time of averaging for each fluorescent spectral pixel Δt=100ms.

Deviations and uncertainties shown in Fig. S8 were found when the time of fluorescent signal collection Δt=100ms. By increasing the averaging time of the instrument, the uncertainty can be decreased. Figure S7 shows an example of such decrease when temperature is fixed at T=20^{o}C.

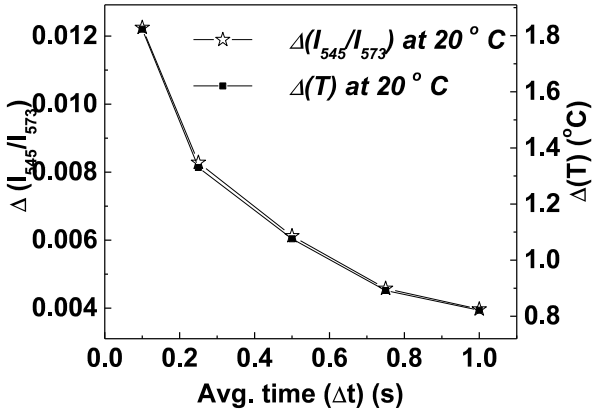

Fig. S8. The dependence of the error of the ratio of intensities on the time of averaging for each spectral fluorescent pixel and corresponding uncertainty in the temperature measurements.

Another important characteristic of the sensors is its stability with respect to multiple changes of temperature. The results of the measurements up to eight full thermal cycles between 20°C and 50°C are shown in Figure S9. One can see a good stability of the synthesized nanothermometers.

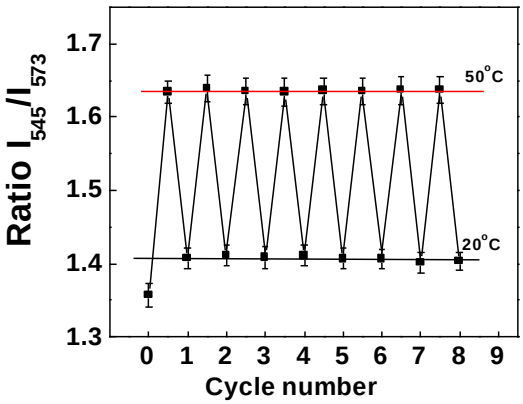

Fig.S9. Stability of the nanothermometers measured up to eight full thermal cycles between 20°C and 50°C.

7. Change in the nanothermometer size after the initial heating

We analyzed the dependence of the particle size on temperature. The particles were initially measured at room temperature (24C) before any heating. Then the particles were heated to 35°C. Then, the particles were cooled back to the room temperature, and heated second time to a higher temperature of 45C. Each time the temperature was stabilized with accuracy of 0.3C before the AFM measurements carried out.

Figure S10 shows a typical height image of nanothermometers and their cross-section.

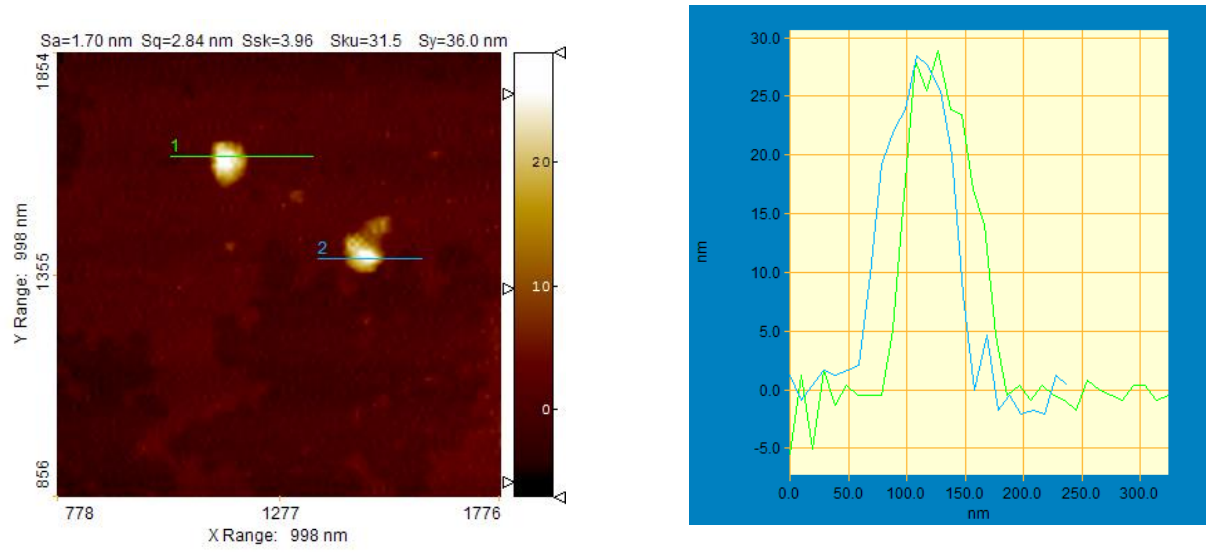

Fig.S10. An example of the AFM images of nanothermometers. A typing AFM image is shown (left). The right panel demonstrates the cross-section of each particle (both vertical and horizontal axes are in nanometers).

The results of the measurements of heights of 5 nanothermometers show that the size of the particles decreases approximately 10-15% after the first thermal cycle and then stay steady. This decrease is due to a well-known completion of condensation of silica from uncondensed hydroxyl groups (Si-OH-) into silica. This process is well described in the literature (see, ref. [5], and also refs. [81, 82] of the main manuscript). It is also worth noting that the size decreases clearly see in comparison of the fluorescence spectra shown in figure S3 (before the heat treatment) and after (figure 3 of the main manuscript). . After shrinkage, the distance between dye molecules

decreases, and consequently, the efficiency of FRET increases. It leads to the diminishing of R6G dye (the donor dye) compared to RB (acceptor dye).

8. Temperature calibration of nanothermometers for the use in 3-D temperature distribution measurements

As a heating source for temperature calibration, the heating stage connecting to a temperature controller (Lakeshore 331) was mounted on the table of the inverted microscope. The hydrogel-nanothermometer sample was placed into specially designed dish and was placed on the heating stage and was preheated to 55 ^{o}C for 30 minutes before proceeding for the actual temperature response. To monitor the temperature of the sample, an IR camera (Therm-App) was used. 2D images were collected in the temperature range of interest and then a temperature profile was obtained. Specifically, temperature versus the fluorescent intensity ratio is shown in Fig.S11.

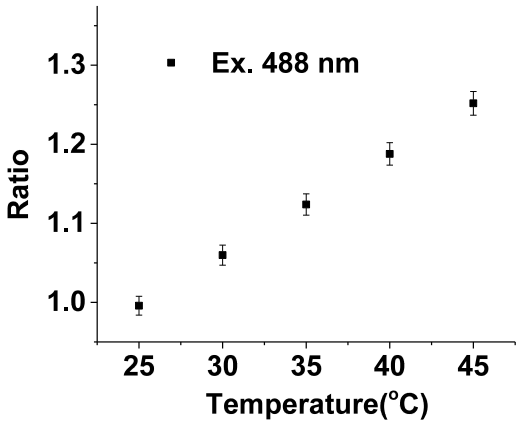

Fig.S11. Temperature dependence of the ratio of fluorescent intensities.

9. COMSOL model to calculate 3-D temperature distribution

To demonstrate an application and working principle of nanothermometers, we measure temperature distribution around a hot wire immersed in hydrogel, as was described in the main text, and as shown in fig. S12. To verify the obtained results with the values predicted by theory, we did numerical simulations using COMSOL Multiphysics software.

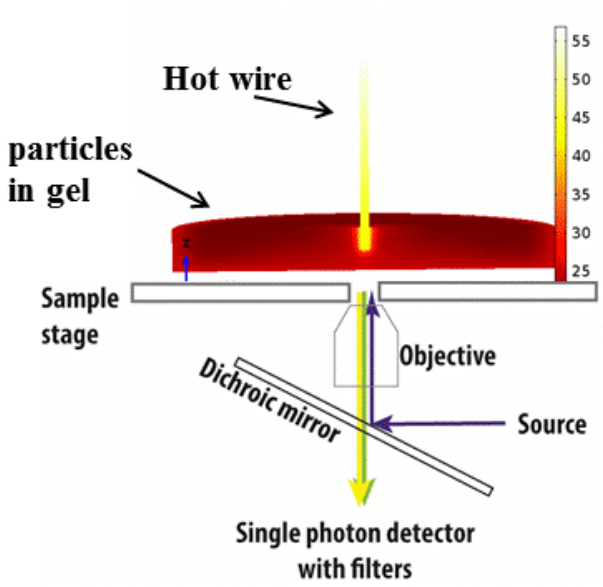

Figure S12. Schematic showing the experimental setup for demonstration of the working principle of nanothermometers

As starting point, we checked whether convection would play a substantial role in the developing of stable temperature distributions; in other word, to check if it is heat transfer problem in which buoyant forces dominate over viscous forces resulting in natural convection [6]. This can be checked by calculating the Grashof number (Gr) given by the following formula

$$Gr = \frac{g\beta(T_s - T_\infty)L^3}{\nu^2}, \qquad \text{(S1)}$$

where g is the acceleration due gravity (9.81 m/s^2), β is the bulk thermal coefficient expansion of the medium (4.57x10^{-4}/K for water), T_s is the temperature of the wire (50 ^{o}C or 323.15 K) , T_∞ is the temperature of the bulk (25 ^{o}C or 298.15K), L is the length of the wire immersed inside the medium(~4.50x10^{-3}m) and ν is the kinematic viscosity (5.53x10^{-7} m^2/s).

One can find that Gr =3400 for the values considered above. It implies that it is a heat transfer problem with natural convection, and thus, the buoyant forces cannot be ignored in the simulations.

Because we performed the experiments after confirming that the setup has reached thermal equilibrium after 30 minutes of the heating the wire (observing steady temperature distribution with IR camera), it is more relevant to simulate for steady state behavior of the system. It should be noted that the steady solution is essentially an average one over time. So, the actual measurements of temperature distribution can fluctuate around the steady solution.

In the COMSOL Multiphysics software, we chose a specific physics interface for the conjugate heat transfer that supports the modeling of heat propagation from solid wire to the liquid. The fluid flow arises due to the temperature dependent local density changes within the fluid, and thus, it is treated as non-isothermal fluid flow. The governing equations that describe the entire phenomenon are the heat balance equation (eq. S2) and the Navier-Stokes (NS) equation (eq. S3). To solve this problem, the continuity equation (conservation of mass) (eq. S4) should be added (for incompressible fluid under steady state conditions). Eq. (S5) gives the volume force, $\mathbf{F}$, which arises due to the change in the fluid densities.

$$\rho C_p \mathbf{u}.\nabla T - \nabla.(\mathrm{k}\,\nabla T) = 0\,, \tag{S2}$$

$$\rho(\mathbf{u}.\nabla)\mathbf{u} = \nabla.\left[-p\,\mathrm{I} + \nabla.\mu(\nabla\mathbf{u} + (\nabla\mathbf{u})^T) - \frac{2}{3}\mu(\nabla.\mathbf{u})\,\mathrm{I}\right] + \mathbf{F}\,, \tag{S3}$$

$$\nabla.(\rho\mathbf{u}) = 0\,, \tag{S4}$$

$$\mathbf{F} = -\mathbf{g}\times(\rho(p,T) - \rho_o)\,. \tag{S5}$$

Here $\mathbf{u}$ velocity vector of the fluid at a given point in the 3D space, ρ, C_p , k and μ are the density and specific heat capacity, thermal conductivity and dynamic viscosity of the fluid, respectively. ρ is considered at a given pressure p and temperature T, and ρ_o in room temperature and pressure (in a non-isothermal fluid flow). **I** here is a unit vector chosen for the brevity of vector representation.

The top end of the wire is was set to 50 ^{o}C temperature, while all other regions of the fluid and the wire was set at 25^{o}C. For the boundary condition of heat transfer, Fig. S13a , we fixed the wire outside the suspension and the open surface of the dish as thermally insulated due to the

fact that the natural convection due to air is assumed to be very small. The dish, which contains the nanothermometer suspension, rests on the base of the inverted microscope that serves as a heat sink. We therefore set the dish bottom at a constant (room) temperature of 25 ^{o}C.

The boundary conditions for the the fluid flow are as follows. Since the fluid is in contact with the dish and the end of the wire (Fig. S13b), a no-slip boundary condition is valid. Since the top portion of the fluid is open to air, we chose a slip condition. The fluid is set to zero velocity as an initial condition in the simulation.

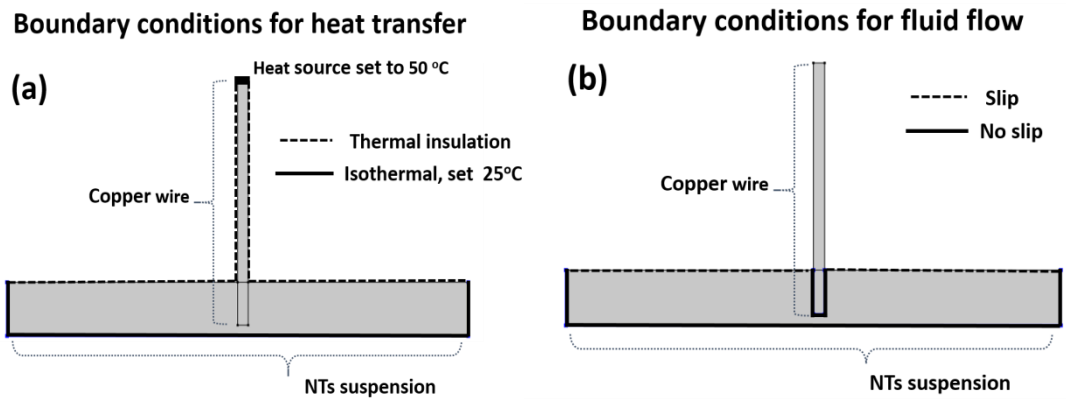

Figure S13: Schematic showing the boundary conditions for heat transfer(a) and boundary conditions for the fluid flow.

10. Temperature measurements of nanothermometers at the single particle level

Figure S14 below shows different regions of interest used to calculate the pixel based integral fluorescence and the background.

Area of interest is 50 x 50 pixels^2:

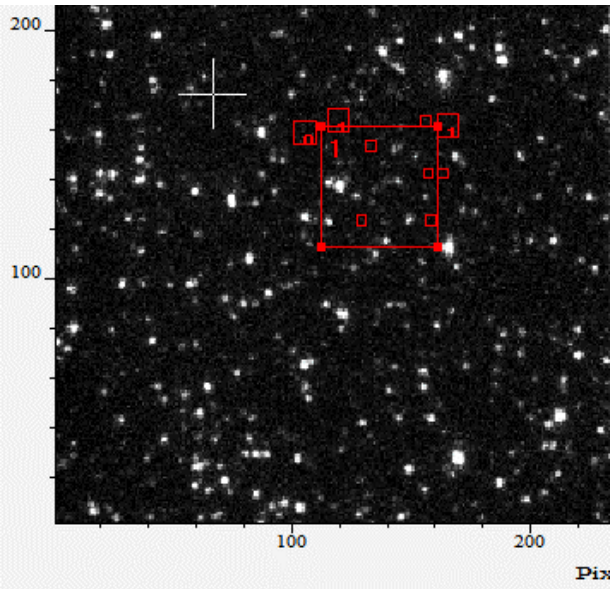

Area of interest is 75 x 75 pixels^2:

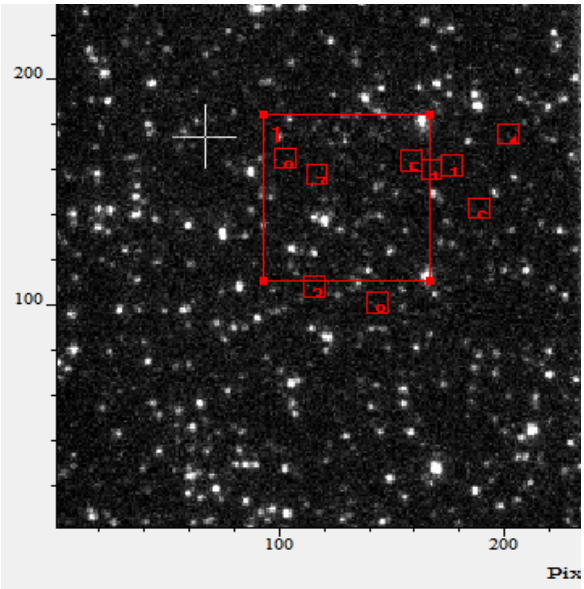

Area of interest is 100 x 100 pixels^2:

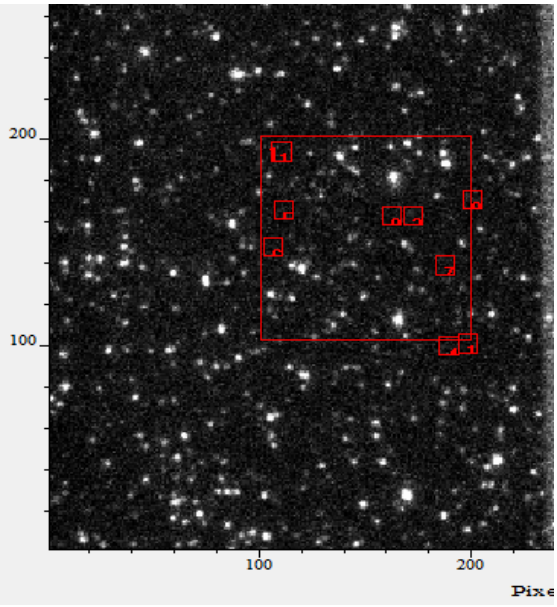

Area of interest is 125 x 125 pixels^2:

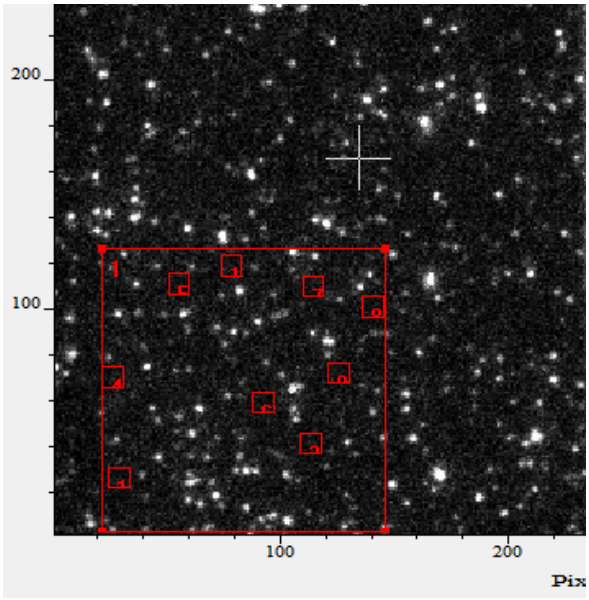

Area of interest is 150 x 150 pixels^2:

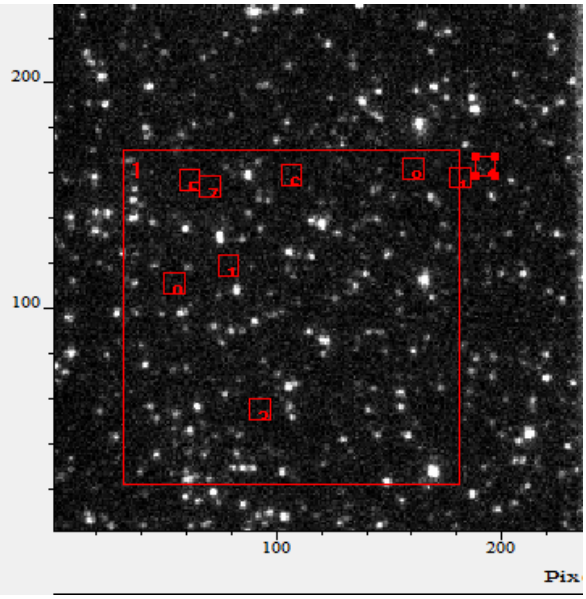

Area of interest is 175 x 175 pixels^2:

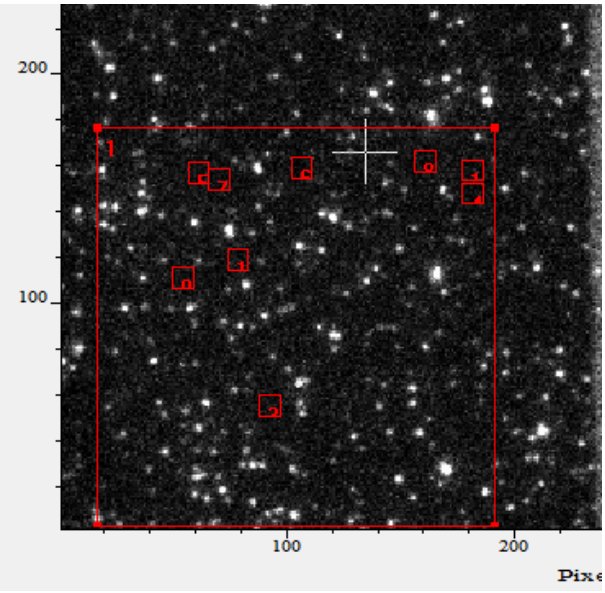

Area of interest is 200 x 200 pixels^2:

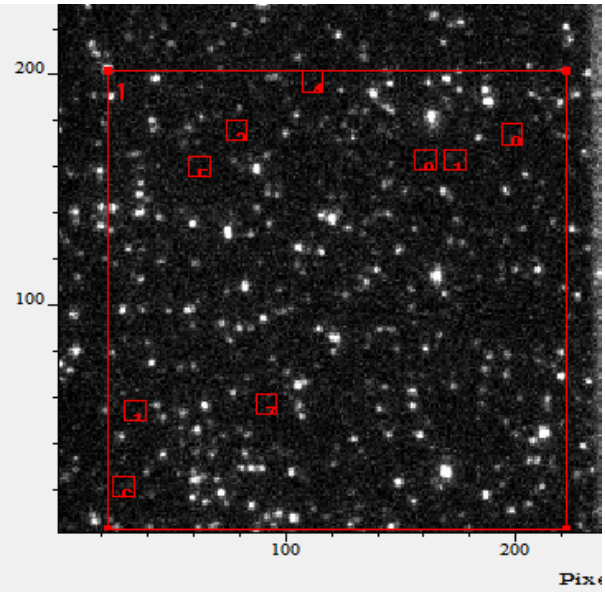

Figure S14: Regions of interests of different area highlighted by large red squares used to calculate the temperature of the entire area. These small squares highlight the regions used to calculate the background.

References

1. Naik, S. P.; Elangovan, S. P.; Okubo, T.; Sokolov, I. *Journal of Physical Chemistry C* **2007,** 111, (30), 11168-11173.
2. Edler, K. J.; Reynolds, P. A.; Whitea, J. W.; Cookson, D. *J. Chem. Soc., Faraday Transactons* **1997,** 93, 199-202.
3. Kalaparthi, V.; Palantavida, S.; Sokolov, I. *J. Mater. Chem. C* **2016,** 4, (11), 2197-2210.
4. Lakowicz, J. R., *Principles of fluorescence spectroscopy*. 3rd ed.; Springer: New York, 2006; p xxvi, 954 p.
5. Iler, R. K., *The chemistry of silica : solubility, polymerization, colloid and surface properties, and biochemistry*. Wiley: New York, 1979; p xxiv, 866 p.
6. Neilson, D. G.; Incropera, F. P. *International Journal of Heat and Mass Transfer* **1991,** 34, (7), 1717-1732.